

# Electrically Driven Formation and Dynamics of Skyrmionic Solitons in Chiral Nematics

Yuan Shen<sup>✉</sup> and Ingo Dierking<sup>✉\*</sup>

*Department of Physics, School of Natural Sciences, University of Manchester, Oxford Road, Manchester M13 9PL, United Kingdom*

 (Received 17 February 2021; revised 31 March 2021; accepted 19 April 2021; published 12 May 2021)

Skyrmions are continuous but topologically nontrivial field configurations that behave like particles. They play an important role in fields ranging from condensed matter to nuclear physics. Realizing and manipulating different kinds of motions of skyrmions are still great challenges. Here, three-dimensional skyrmions, in the form of double-twist tori terminated on two topological point defects called “torons,” are produced in chiral nematic liquid crystals with varied helical pitches. The spontaneous formation of skyrmions and high-degree multiskyrmion configurations called “skyrmion bags” are characterized by polarizing microscopy. The skyrmions show anomalous diffusion in the equilibrium state and perform collective directional motion driven by fluid flows, with a velocity controllable by electric fields and surface anchoring. They can be utilized as vehicles for microcargo transport. We also show that skyrmions can collide and form clusters with tunable shape, anisotropy, and fractal dimension.

DOI: [10.1103/PhysRevApplied.15.054023](https://doi.org/10.1103/PhysRevApplied.15.054023)

## I. INTRODUCTION

Solitons are self-sustained localized packets of light or matter waves in nonlinear media that propagate without changing shape. They are ubiquitous and exist in various areas of physics, such as nonlinear photonics, hydrodynamics of fluids, plasma, superconductors, magnetic materials, and liquid crystals (LCs) [1,2]. Topological solitons, as a very different kind of soliton, are topologically nontrivial field configurations embedded in a uniform far-field background that behave like particles and cannot be transformed into a uniform state through smooth deformations [3]. They emerge in theories that span many branches of physics, such as the instantons in quantum theory, vortices in superfluids, and rotons in Bose-Einstein condensates, and have attracted much attention from physicists and mathematicians. The beginnings go back to Gauss, who envisaged that localized knots of physical fields could behave like particles [4,5]. As a primitive model of atoms, Kelvin suggested that various chemical elements could be represented by knotted vortices [3]. Later, Skyrme developed a nonlinear theory of pions in three spatial dimensions, which could model elementary particles with different baryon numbers as topological solitons with different topological degrees [6,7]. Due to the universality of their mathematical models and physical structures, solitons with similar topological configurations can emerge in different physical systems with their physical properties being related. In condensed matter physics, low-dimensional

Skyrme solitons (introduced as “baby skyrmions”) have been experimentally investigated in magnets [8,9] and LCs [10,11], with the former showing promise for racetrack memory and spintronic devices [12] and the latter for various optical applications [13–15].

Nematic LCs are self-organized anisotropic fluids with long-range orientational order of elongated molecules defined by the average of the long molecular axis called the director,  $\mathbf{n}$ . They have been an ideal testbed for investigations of various soliton phenomena since the 1960s, which started with studies of static linear and planar solitons induced by magnetic or electric fields [16,17]. By rotating the applied fields, a variety of interesting behaviors of these solitons were subsequently reported [18–20]. Propagating solitary waves can be generated in nematics by shearing the samples [21–23]. Nematicons, which represent self-focused continuous-wave light beams in nematic LCs, are well known for their potential applications in optical information technology [24]. Recently, three-dimensional (3D) dynamic dissipative solitons were reported in nematics that showed various exotic dynamic behaviors and received much attention [25–29]. Furthermore, a number of topological solitons are observed in chiral nematic LCs (CNLCs). In a ground-state CNLC,  $\mathbf{n}$  twists continuously along a helical axis perpendicular to the local long molecular axis at a constant rate. The distance over which  $\mathbf{n}$  rotates by  $2\pi$  is named “pitch,”  $p$  [30,31]. This helical structure of a CNLC can be deformed by applying electric fields or by confining it between surfaces with homeotropic anchoring, leading to geometric frustration, which is usually locally relieved by forming

\*ingo.dierking@manchester.ac.uk

topological defects [32]. Depending on the strength of applied fields or anchoring, these defects may be relaxed into stringlike structures called cholesteric fingers [33] or nonsingular solitonic structures called cholesteric bubbles or spherulitic domains [34]. It was not recognized until recently that these cholesteric bubbles were, in fact, topological analogs of skyrmions [35,36]. These skyrmionic structures can be stabilized as individual particlelike excitations and arranged into crystalline arrays and linear chains [13,37]. They are usually investigated as static field configurations [35,38], with only a few studies being related to their out-of-equilibrium dynamics [39]. Dynamic motion of skyrmions is of paramount interest for applications such as information storage in magnets [12] and microfluidics in LCs [27]. Despite the fact that electrically driven motion of skyrmions has been recently reported in both magnets [40] and LCs [39], realizing different kinds of motions and manipulating these motions are still topics of significant challenge.

In this work, topological solitons of elementary two-dimensional (2D) skyrmions capped by two 3D singular point defects (“Bloch points” in the magnetic analogy [41]) called “torons” or “hopfions” [38] are generated in CNLCs confined between surfaces with homogeneous anchoring by applying electric fields, which were previously studied only in homeotropic confinement [11,34]. By changing the ratio of the thickness of LC cells,  $d$ , and the pitch,  $p$ , of CNLCs, topological solitons exhibit different optical textures and dynamic behaviors. The formation process of the solitons is characterized and demonstrated in detail. In addition, the spontaneous formation of so-called “skyrmion bags,” with a tunable topological degree is also demonstrated, which may enlighten approaches in encoding information in both optical and magnetic information storage. We find that these topologically protected skyrmionic solitons undergo anomalous diffusion at equilibrium and perform collective directional motion in nonequilibrium states. Their velocity can be controlled by tuning the electric field and surface anchoring, enabling fascinating dynamic behaviors. Interestingly, they can even be utilized as vehicles for directed micro-cargo transport. Furthermore, we also induce skyrmionic solitons in systems of high chirality and show that they behave like colloidal particles and exhibit various exotic dynamic behaviors. They can even form clusters with tunable shape, anisotropy, and fractal dimension during inelastic collisions, which may enable mesostructured soft-matter composites with tunable mechanical and optical properties.

## II. RESULTS

### A. Structure and formation of skyrmionic solitons ( $d/p \sim 3.9$ )

Torons are embedded in the background of a quasi-homeotropic director field and are stabilized by an

intermediate-strength electric field [Figs. 1(a) and 1(b)]. The structure of a toron is derived from its optical textures [Fig. 1(a)], which can be represented by a baby skyrmion, featuring a  $\pi$  radial twist from its center to periphery stabilized by the strong energy barriers associated with the nucleation of two hyperbolic defects at its ends [Figs. 1(c) and 1(d)]. The point defects of opposite hedgehog charges facilitate transformation of the soliton to a topologically trivial uniform state. In cases with homeotropic boundaries, the two point defects usually nucleate near the boundary surfaces [11,36]. However, in our case, we presume that the torons are located in the middle layer of the cell with the point defects away from the boundary surfaces due to the large ratio of cell gap and pitch ( $d/p \sim 3.9$ ). It is found that the torons cannot be stabilized in a system with  $d/p \sim 1$ , which may be due to the incompatibility of the point defects with homogeneous anchoring. For nonpolar director fields ( $\mathbf{n} = -\mathbf{n}$ ), such a toron can be regarded as a baby skyrmion and can be labeled by elements of the second homotopy group,  $\pi_2(S^2/Z_2) = Z$ , and its topological degree,  $Q$ , can be represented by the skyrmion number that counts the integer number of times the order parameter space,  $S^2/Z_2$ , is covered by its director field [Figs. 1(c) and 1(d)] [42]. In our experiment, the configuration of the sample is similar to that in LC displays, where the CNLC is confined between two conductive glass substrates with homogeneous alignment. The  $x$  axis indicates the alignment direction, and the electric field is applied along the  $z$  axis (Fig. 1). The sample first shows a typical fingerprint texture [43], Fig. 1(b). By increasing the amplitude of the electric field,  $E$ , the fingers gradually shrink due to the unwinding effect [30]. Each finger shortens symmetrically from its two ends, and it is found that a toron forms when the two ends meet [Fig. 2(a)]. These fingers are topologically equivalent to torons and are classified as second-type cholesteric fingers (CF2) [44,45]. We find these CF2s can drift with a constant velocity in a direction perpendicular to their long axes [46] and form dynamic spirals [47] at low frequency,  $f$  (Fig. S1 within the Supplemental Material [48]), which is attributed to Lehmann rotation and flexoelectric effects [46]. First-type fingers (CF1s) are observed in thinner cells and can crawl in a direction parallel to their long axes (Fig. S1 within the Supplemental Material [48]), yet they cannot form solitons [47]. On the other hand, some fingers also form closed loops, which continuously shrink and eventually form topological solitons [Fig. 2(b)]. It is noted that the solitons formed from the loops have a larger diameter than the ones formed directly from fingers, with a slightly different texture. This may indicate that they have different topological structures, which requires further investigation. Moreover, sometimes a soliton may even form inside a loop that constitutes a skyrmion bag [49]. However, such a configuration is not stable: the center soliton will get squeezed and annihilate, and the loop will collapse into a single soliton within seconds [Fig. 2(c)]. Interestingly, such transformations are

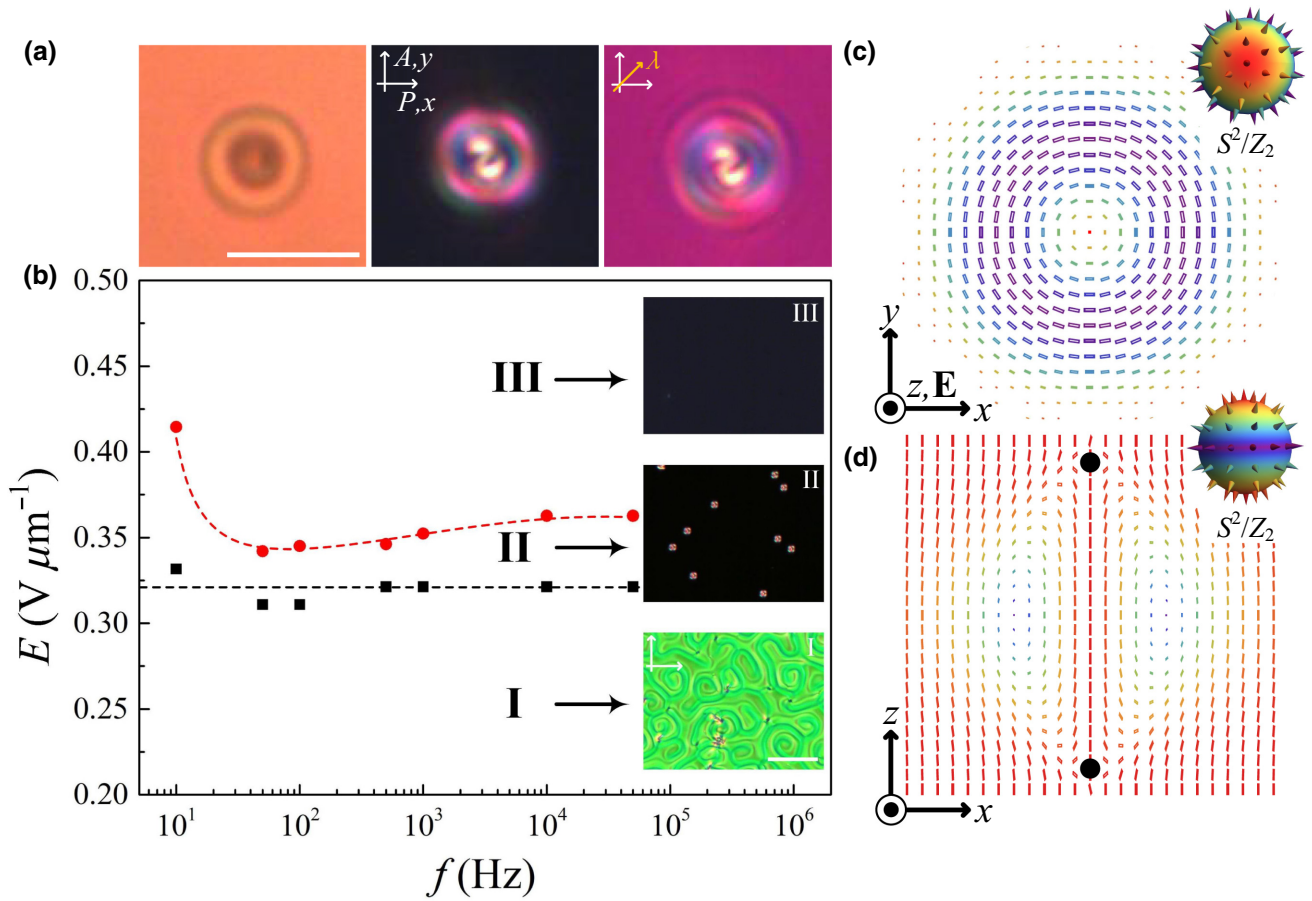


FIG. 1. Skyrmionic solitons in CNLCs with pitch  $p \sim 5 \mu\text{m}$  confined in a cell with cell gap  $d = 19.3 \mu\text{m}$ . (a) From left to right, micrographs of a soliton ( $E = 0.33 \text{ V } \mu\text{m}^{-1}$ ,  $f = 50 \text{ kHz}$ ) without polarizers; with crossed polarizers; with crossed polarizers and a first-order red plate compensator (530 nm), the slow axis of which,  $\lambda$ , makes an angle of  $45^\circ$  with the crossed polarizers. Scale bar  $10 \mu\text{m}$ . (b) Threshold dependence of different states (I, fingerprint textures; II, soliton state; III, quasihomotropic state) on the frequency of an applied rectangular ac electric field,  $f$ . Insets are the polarizing micrographs of different states (I,  $E = 0 \text{ V } \mu\text{m}^{-1}$ ; II,  $E = 0.33 \text{ V } \mu\text{m}^{-1}$ ;  $f = 50 \text{ kHz}$ ; III,  $E = 0.36 \text{ V } \mu\text{m}^{-1}$ ,  $f = 50 \text{ kHz}$ ). Scale bar  $50 \mu\text{m}$ . White arrows indicate polarizers. Director configuration of a soliton in the  $x$ - $y$  plane (c) and  $x$ - $z$  plane (d), where  $\mathbf{n}$  is represented as rods colored according to their orientations on target  $S^2/Z_2$  sphere (insets).

even reversible, i.e., the solitons formed from loops can transform into loops, while the ones formed from fingers turn into fingers [Figs. 2(d) and 2(e), Movie S1 within the Supplemental Material [48]]. A further increase of  $E$  will destroy these topologically protected configurations and lead to a cholesteric-nematic phase transition [Fig. 1(b)].

### B. Formation of skyrmion bags ( $d/p \sim 3.9$ )

Higher-degree skyrmion configurations are attractive to researchers due to their potential applications for high-density information storage [9,50]. It was reported that such high-degree skyrmion configurations, also called skyrmion bags, could be realized in CNLCs by laser tweezers [49,51]. Here, we show that these skyrmion bags can also form spontaneously by relaxing electrohydrodynamic

instabilities. Compared with laser tweezers, the application of electric fields is more flexible and convenient. In addition, as an analog of magnetic skyrmions, it is also more practical and acceptable for applications in information storage. Figure 3(a) shows skyrmion bags  $S(1)$  to  $S(4)$ ,  $S(16)$ , and  $S(29)$ , which are stabilized by a low-frequency modulated electric field. As reported in Ref. [49], we denote skyrmion bags as  $S(N_S)$ , where  $N_S$  is the number of (anti)skyrmions inside the large bag skyrmion. However, unlike the skyrmion bags reported in Ref. [49], where the bag skyrmion is formed by twisted wall loops and has a topological degree of  $Q = -1$ , the bag skyrmion, in our case, is formed by a looped CF2 with  $Q = 2$  [47,49]. Hence, the total topological degree,  $Q$ , of a skyrmion bag  $S(N_S)$  in our case is  $N_S + 2$ . In Fig. 3(b), we demonstrate that the topological degree of a skyrmion bag can be

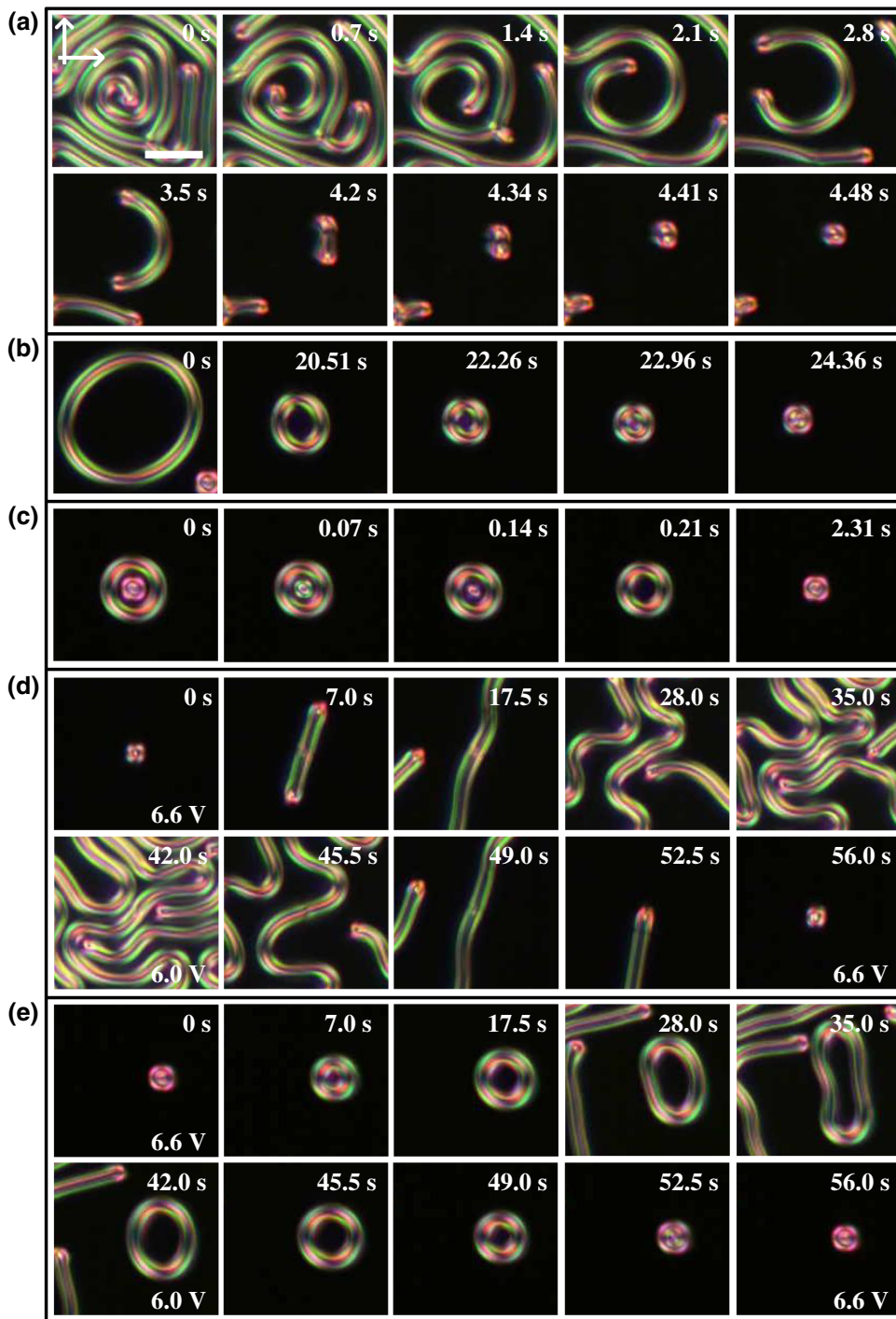


FIG. 2. Formation of skyrmionic solitons in CNLCs with pitch  $p \sim 5 \mu\text{m}$  confined in a cell with cell gap  $d = 19.3 \mu\text{m}$ . (a) Shrinking of a cholesteric finger into a soliton ( $U = 6.6 \text{ V}$ ,  $f = 50 \text{ kHz}$ ). (b) Collapse of a looped cholesteric finger into a soliton ( $U = 6.6 \text{ V}$ ,  $f = 50 \text{ kHz}$ ). (c) Collapse of a skyrmion bag into a single soliton ( $U = 6.6 \text{ V}$ ,  $f = 50 \text{ kHz}$ ). (d) Reversible transformation between a soliton and a cholesteric finger. (e) Reversible transformation between a looped cholesteric finger and a soliton. In (d),(e),  $U$  gradually changes from 6.6 to 6.0 then to 6.6 V,  $f = 50 \text{ kHz}$ . Scale bar  $20 \mu\text{m}$ . White arrows indicate polarizers.

changed by simply tuning the frequency, where  $Q$  changes continuously from 7 to 16 and then from 16 to 23 (Movie S2 within the Supplemental Material [48]). Figure 3(c) shows the reversible transformation between a skyrmion bag and cholesteric fingers with constant  $Q$ . Finally, we show that these skyrmion bag configurations can also be easily cleared. In Fig. 3(d), a bag skyrmion is cut by a soliton located outside, leading to the annihilation of the outer soliton and the transformation of the bag skyrmion to a single soliton (yellow dashed circle).

### C. Brownian motion of skyrmionic solitons ( $d/p \sim 2.6$ )

The dynamics of topological solitons is investigated in the system with a smaller pitch of  $p \sim 2 \mu\text{m}$ . It is found that, although sharing the same field configurations, the polarizing optical textures of torons of different pitches are different (Fig. 1, Fig. S2 within the Supplemental Material [48]), which is due to the different phase retardations and rotations of polarization when light is traversing through the samples with different  $d/p$  ratios [52]. It is also found

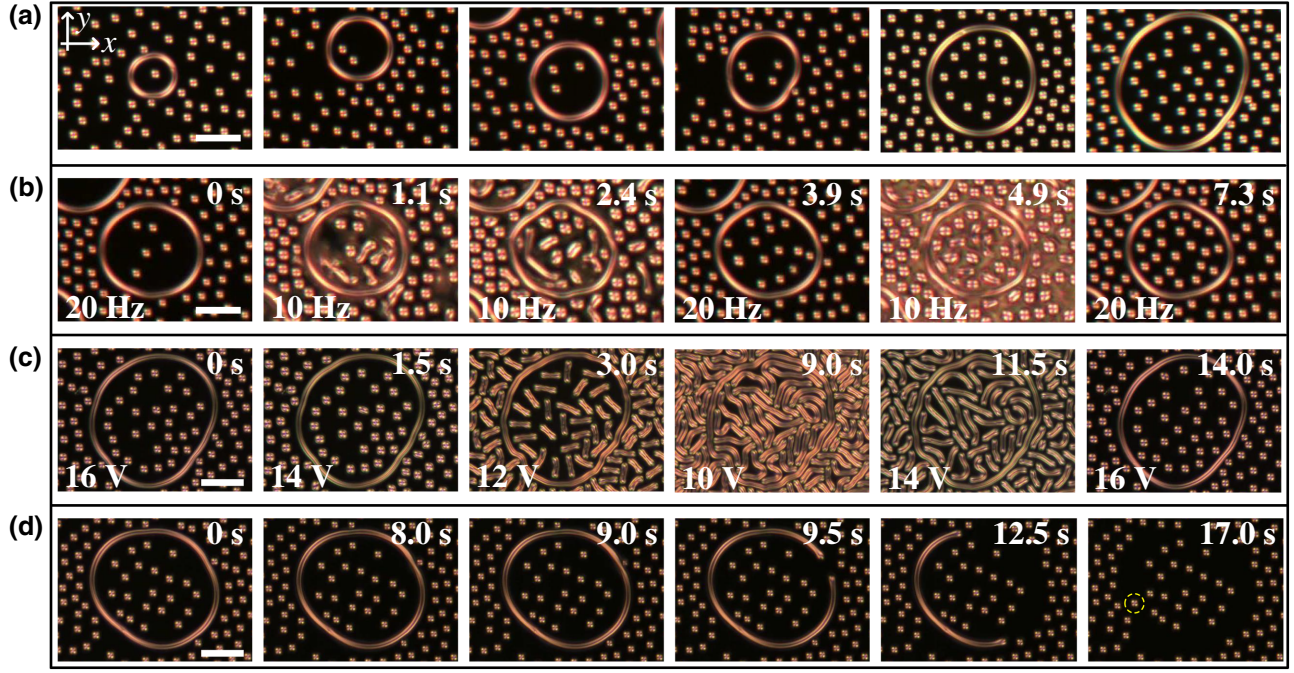


FIG. 3. Skyrmion bags in CNLCs with pitch  $p \sim 5 \mu\text{m}$  confined in a cell with cell gap  $d = 19.3 \mu\text{m}$ . (a) Polarizing micrographs of skyrmion bags  $S(1)$  to  $S(4)$  ( $U = 16.0 \text{ V}, f = 50 \text{ kHz}, f_m = 20 \text{ Hz}$ ),  $S(16)$ , and  $S(29)$  ( $U = 12.0 \text{ V}, f = 50 \text{ kHz}, f_m = 30 \text{ Hz}$ ). (b) Changing the topological degree of a skyrmion bag by tuning electric field ( $U = 16.0 \text{ V}, f = 50 \text{ kHz}$ ;  $f_m$  is indicated in the bottom left of each figure). (c) Reversible transformation between skyrmions and cholesteric fingers ( $f = 50 \text{ kHz}, f_m = 20 \text{ Hz}$ ;  $U$  is indicated in the bottom left of each figure). (d) Transformation of a bag skyrmion into a skyrmionic soliton ( $f = 50 \text{ kHz}, f_m = 20 \text{ Hz}$ . From left to right,  $U$  increases gradually from 16.0 to 18.0 V. Scale bars  $50 \mu\text{m}$ . Polarizer and analyzer are parallel to the  $x$  and  $y$  axis, respectively.

that it requires higher applied electric fields,  $E$ , to induce the torons, which is due to the larger twist energy of CNLCs with smaller pitch ( $F_T = K_2 q[\mathbf{n} \cdot (\nabla \times \mathbf{n})]$ , where  $K_2$  is the twist elastic constant,  $q = \pi/p$ ) [30] (Fig. S2 within the Supplemental Material [48]). The solitons undergo Brownian motion at equilibrium, just like colloidal particles. Translational diffusion of solitons is driven by the localized thermal fluctuations of  $\mathbf{n}$  and is resisted by the LC's viscous drag associated with rotational viscosity  $\gamma$ . Figure 4(a) shows the dependences of the mean squared displacement (MSD) of a colloidal microparticle, a soliton, and an immobile particle, on time lag  $\tau$ . The MSD of the particle grows linearly with  $\tau$ :  $\langle \Delta r^2(\tau) \rangle = 6D\tau$ , where  $D$  is the diffusion coefficient [53,54]. Interestingly, the soliton exhibits anomalous behavior,  $\langle \Delta r^2(\tau) \rangle \propto \tau^\alpha$ , with exponents  $\alpha_x = 0.83$  and  $\alpha_y = 0.48$  [Fig. 4(b), inset], where  $\alpha_x$  and  $\alpha_y$  are the exponents in the  $x$  and  $y$  directions, respectively. Such a subdiffusion regime can better be visualized with the velocity autocorrelation function,  $C_{vx}(\tau) = \langle v_x(\tau)v_x(0) \rangle$ , where  $v_x$  is the velocity of the soliton along the  $x$  axis and, similarly,  $C_{vy}(\tau) = \langle v_y(\tau)v_y(0) \rangle$  for the  $y$  direction [55,56]. In Fig. 4(b), it is found that both  $C_{vx}$  and  $C_{vy}$  are negative for short timescales, indicating subdiffusion. Furthermore, such diffusion is found to be dependent on voltage [Figs. 4(c) and 4(d)]. One can thus determine the half-width  $\Delta$  of the histograms of displacements by

fitting the data with Gaussians. The diffusivity of the soliton,  $D = \Delta^2/\tau$ , and thus, the effective viscous drag coefficients can be calculated according to Einstein's relation  $\xi = k_B T/D$ , where  $k_B = 1.38 \times 10^{-23} \text{ J K}^{-1}$  is Boltzmann's constant and  $T$  is the absolute temperature [53]. It is found that  $D$  slightly increases for increasing voltage ( $U$ ) and saturates at  $U = 5.5 \text{ V}$  (Table S1 within the Supplemental Material [48]), which may be attributed to the negative correlation between the diameter of solitons and applied voltages (Fig. S3 within the Supplemental Material [48]).

#### D. Coherent directional motion of skyrmionic solitons ( $d/p \sim 2.6$ )

On the other hand, directional collective motion of torons can be induced by applying an electric field modulated with a low frequency,  $f_m$  [Fig. 5(a)]. Figure 4(e) shows different states of the CNLC by varying the modulated electric field. It is found that, besides the torons, dynamic dissipative solitons are also induced at low  $f_m$ . Such dissipative solitons were recently reported by us [28] and are induced by the nonlinear coupling between the director field and the isotropic flow of ions. Unlike torons, they can exist only under nonequilibrium conditions. In contrast, the torons can drift (perpendicular to the alignment direction,  $y$  axis) over a wide range of modulation

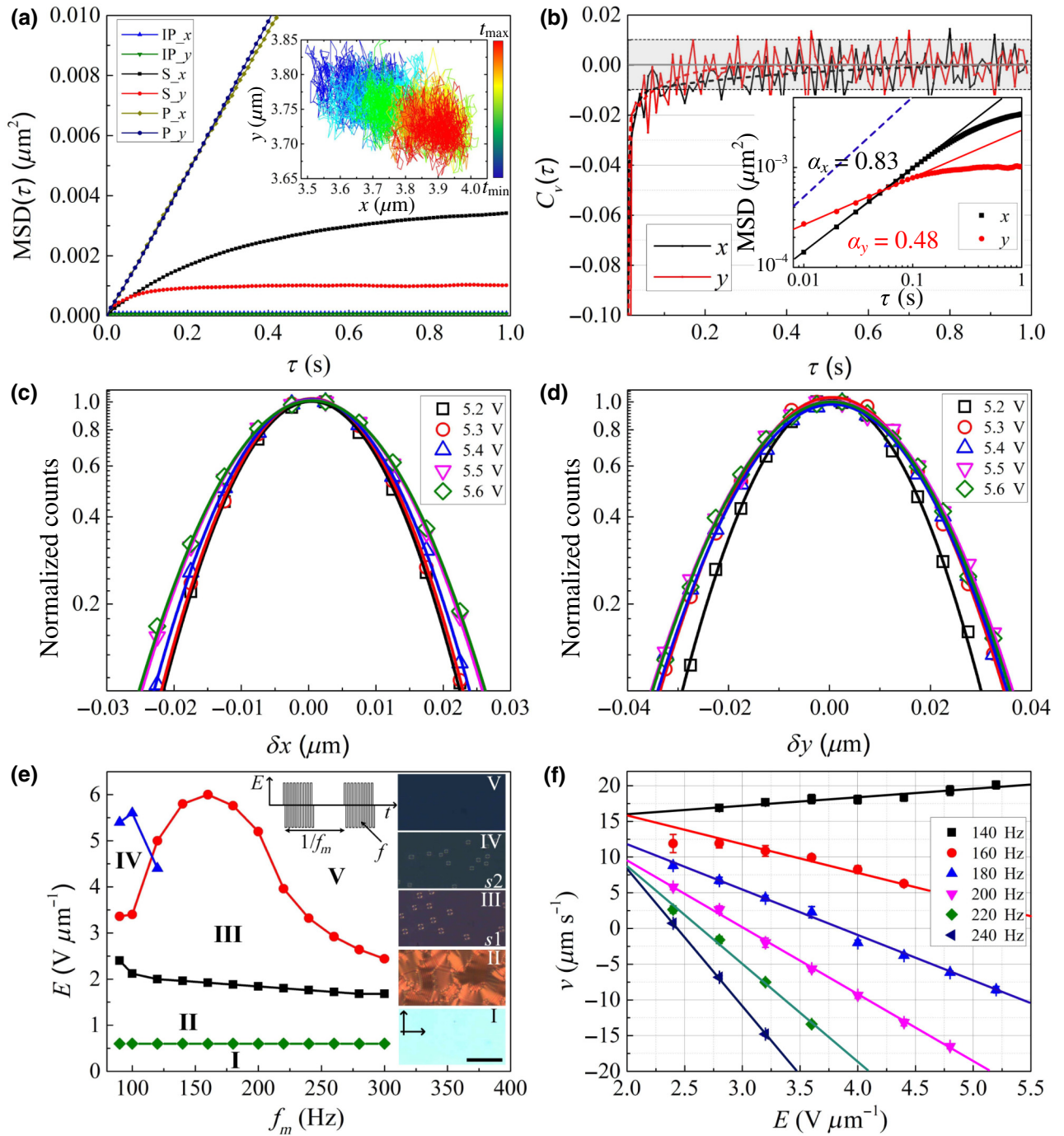


FIG. 4. Dynamics of skyrmionic solitons in CNLCs with pitch  $p \sim 2$   $\mu\text{m}$  confined in a cell with cell gap  $d = 5.1$   $\mu\text{m}$ . (a) MSDs versus time lag  $\tau$  of an immobile particle (IP), a soliton (S), and a colloidal particle (P) in the direction parallel ( $x$ ) and perpendicular to ( $y$ ) the alignment direction. Inset shows the trajectory of the soliton with time corresponding to the color bar,  $t_{\min} = 0$  s,  $t_{\max} = 100$  s. (b) Velocity autocorrelation functions for the soliton diffusing along  $x$  and  $y$  axes, respectively. Dashed lines (black and red) are polynomial fits. Inset shows the  $\log_{10}$ - $\log_{10}$  plot of MSD versus  $\tau$  of the soliton. Blue dashed line indicates a slope of one for reference. Histograms of displacement of the soliton (c) along the  $x$  axis and (d) along the  $y$  axis at different  $U$  for time lag of 10 ms; solid lines are Gaussian fits of experimental data points (open symbols, data of the soliton at each voltage are obtained from 30 000 trajectory steps). (e) Threshold dependence of different states [I, homogeneous state; II, fingerprint texture; III, dynamic topological soliton state ( $s_1$ ); IV, dissipative soliton state ( $s_2$ ); V, quasihomotropic state] on modulated electric field frequency,  $f_m$ . Profile of modulating electric field is indicated as an inset. Insets (I–V) are polarizing micrographs of different states (I,  $E = 0$   $\text{V } \mu\text{m}^{-1}$ ; II,  $E = 1.18$   $\text{V } \mu\text{m}^{-1}$ ,  $f_m = 140$  Hz; III,  $E = 2.75$   $\text{V } \mu\text{m}^{-1}$ ,  $f_m = 140$  Hz; IV,  $E = 2.75$   $\text{V } \mu\text{m}^{-1}$ ,  $f_m = 100$  Hz; V,  $E = 6.0$   $\text{V } \mu\text{m}^{-1}$ ,  $f_m = 140$  Hz),  $f = 50$  kHz. Scale bar  $50$   $\mu\text{m}$ . Black arrows indicate crossed polarizers. (f) Dependence of amplitude of velocity,  $v$ , of topological solitons on amplitude of modulated electric field,  $E$ ; solid lines are linear fits of experimental data points (symbol). Error bars of each data point are calculated from standard deviation of velocities of hundreds of different solitons at same electric field.

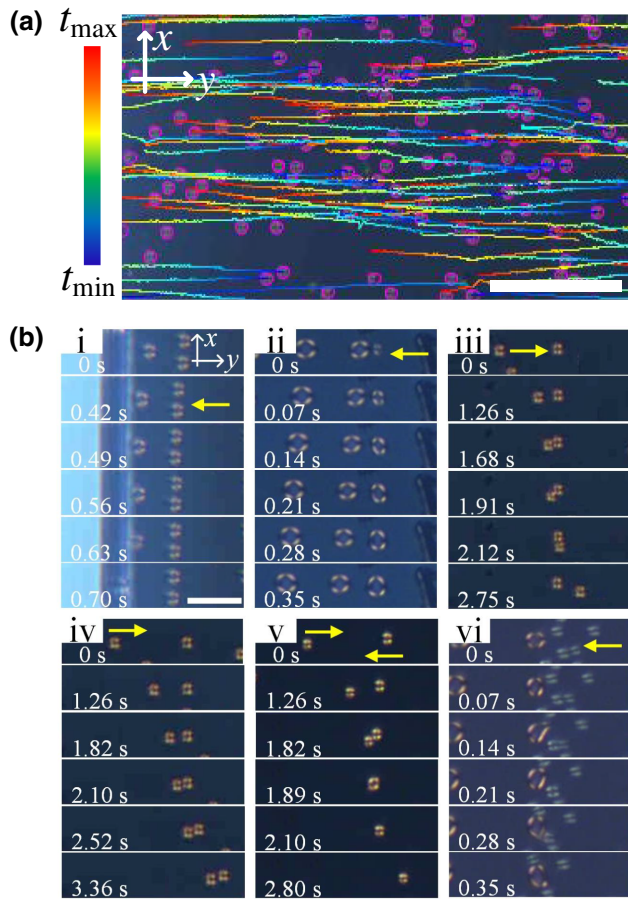


FIG. 5. Collective motion and interactions of skyrmionic solitons in CNLCs with pitch  $p \sim 2 \mu\text{m}$  confined in a cell with cell gap  $d = 5.1 \mu\text{m}$ . (a) Trajectories of skyrmionic soliton motions with time, according to the color bar ( $t_{\min} = 0 \text{ s}$ ,  $t_{\max} = 20 \text{ s}$ ). Scale bar  $60 \mu\text{m}$ .  $E = 2.75 \text{ V } \mu\text{m}^{-1}$ ,  $f = 50 \text{ kHz}$ ,  $f_m = 180 \text{ Hz}$ . Polarizer and analyzer are parallel to  $x$  and  $y$  axes, respectively. (b) Interactions of skyrmionic solitons: i, solitons disappear at the electrode edge ( $E = 2.35 \text{ V } \mu\text{m}^{-1}$ ,  $f = 50 \text{ kHz}$ ,  $f_m = 200 \text{ Hz}$ ); ii, solitons nucleate at a surface imperfection ( $E = 3.53 \text{ V } \mu\text{m}^{-1}$ ,  $f = 50 \text{ kHz}$ ,  $f_m = 130 \text{ Hz}$ ); iii, moving soliton collides with a soliton pinned at a dust particle ( $E = 2.35 \text{ V } \mu\text{m}^{-1}$ ,  $f = 50 \text{ kHz}$ ,  $f_m = 180 \text{ Hz}$ ); iv, moving soliton collides with an immobile soliton and both move together ( $E = 2.35 \text{ V } \mu\text{m}^{-1}$ ,  $f = 50 \text{ kHz}$ ,  $f_m = 180 \text{ Hz}$ ); v, two solitons moving in opposite directions collide and one of them is absorbed by the other ( $E = 2.35 \text{ V } \mu\text{m}^{-1}$ ,  $f = 50 \text{ kHz}$ ,  $f_m = 220 \text{ Hz}$ ); vi, absorption of dissipative solitons by a topological soliton ( $E = 2.75 \text{ V } \mu\text{m}^{-1}$ ,  $f = 50 \text{ kHz}$ ,  $f_m = 130 \text{ Hz}$ ).

frequencies,  $f_m$ , with a velocity that can be controlled by the applied electric field [Fig. 4(f), Movies S3 and S4 within the Supplemental Material [48]]. Such motion is somewhat similar to the schools of skyrmions reported recently [57], but with a much larger velocity. We attribute this motion to the coupling between backflow and the squirming motion of torons. Due to the positive dielectric anisotropy,  $\mathbf{n}$  tends to orient parallel to the electric field

direction. At low  $f_m$ ,  $\mathbf{n}$  periodically rotates from its initial horizontal orientation to a vertical orientation. Such a nonreciprocal rotational dynamics of  $\mathbf{n}$  induces the backflow that drives the torons. At the same time, the twisted region is squeezed and relaxed as the voltage is applied and turned off, within  $1/f_m$ , making the torons expand, contract, and morph as they move [39], resembling the squirming motion of active microswimmers [58]. By tuning  $E$  and  $f_m$ , the torons can alter their motion direction reversibly between the  $+y$  and  $-y$  directions [Fig. 4(f), Movie S5 within the Supplemental Material [48]]. It is well known that the velocity profile of backflow in homogeneous confinement is bidirectional, i.e., the velocity field in the top half of the cell is an inverse mirror image of the one in the bottom half [59]. Tuning the electric field may induce a positional transition of torons [60,61], thus leading to such a bidirectional reversal of motion. Figure 5(b) shows various dynamic interactions among torons during motion. It is observed that the skyrmionic solitons disappear once they move to the electrode [Fig. 5(b), i], which is different from the dissipative solitons reported previously, where reflection of solitons was observed [27]. However, the skyrmionic solitons can nucleate at irregularities, such as surface imperfections and dust particles [Fig. 5(b), ii], which is similar to dissipative solitons [27]. The skyrmionic solitons collide with each other like particles during motion. In Fig. 5(b), iii, a moving soliton collides with an immobile soliton, which is trapped by a dust particle, and then moves away from the immobile soliton. On the other hand, if the immobile soliton is not trapped, it is pushed by the moving soliton and starts moving itself [Fig. 5(b), iv]. More interestingly, it is found that, at some specific frequencies and voltages, there are “two kinds” of solitons, i.e., large ones that move more slowly towards the left and smaller ones that move more quickly towards the right. The number of small solitons is much smaller than that of the large ones. During motion, the small soliton is absorbed by the large one, if they collide with each other. After the collision, the larger one continuously shrinks into a small soliton and moves in the opposite direction at a higher speed (v, Movie S3 within the Supplemental Material [48]). The reason for such behavior and the differences between the topological structures of these two kinds of solitons are not clear yet and require further investigation. One possible assumption is that these two kinds of solitons are actually topologically equivalent. However, the smaller ones are somehow located at a higher energy level, maybe due to the drastic symmetry breaking of the LC phase induced by the steep increase of applied voltage. The reason why this is believed is that the optical texture and dynamic behaviors (speed and moving direction) of the small solitons are very similar to the large ones at higher voltages. Furthermore, at low  $f_m$ , dissipative solitons are induced and are absorbed by the skyrmionic solitons once they interact with each other [Fig. 5(b), vi].

Details of these interactions can be found in Movie S6 within the Supplemental Material [48].

In previous studies [11,34,52,62], the skyrmions are always confined between surfaces with homeotropic anchoring, and thus, their direction of motion is randomly determined by the spontaneous symmetry-breaking structures [39] or many-body interactions [57]. Here, by using homogeneous alignment, the direction of motion of the torons can be easily controlled. In Fig. S4(a) within the Supplemental Material [48], a sample is divided into regions with different alignment directions through the photoalignment technique [63]. It is found that the torons move perpendicular to the predesigned alignment direction in each region. Once they reach the border of the region, they are absorbed by disclinations formed in the border regions. Interestingly, it is found that there is a disclination splitting the left region into two subregions. Such a disclination is formed from the high-field-induced collapse of a  $\pi$  wall [a planar soliton is represented by the first homotopy group,  $\pi_1(S^2/Z_2) = Z_2$ ]. The director thus twists  $\pi$  from the left to the right subregion, leading to the motion of torons in opposite directions (Movie S7 within the Supplemental Material [48]). Furthermore, it is reported that localized distortions of director fields can attract colloidal particles to minimize the elastic free energy [31,64]. As a result, we show that these soliton structures can be utilized as vehicles for microcargo transport. In Fig. S4(b) within the Supplemental Material [48], a toron is induced near an aggregate of two microparticles by applying an electric field and then carries these, while moving through the nematic bulk. More importantly, such a process is repeatable, and the speed and trajectory of transport is also controllable by tuning the electric field and surface anchoring (Movie S8 within the Supplemental Material [48]).

### E. Dynamics of skyrmionic solitons with high chirality ( $d/p \sim 13.3$ )

To investigate the influence of chirality, skyrmionic solitons are induced in CNLCs with a much smaller pitch ( $p \sim 0.375 \mu\text{m}$ ) compared with previous investigations. In addition to the smaller size and higher  $E$  threshold, compared with those with larger pitch  $p$ , the skyrmionic solitons in this case have an inhomogeneous diameter distribution (Fig. S5 within the Supplemental Material [48]). It is found that, during the formation of solitons, unstable skyrmion bags with different  $N_S$  are formed randomly. Unlike the skyrmion bags mentioned above, the loops discussed here shrink and absorb the solitons inside, thus forming solitons with extraordinarily large diameters (Fig. S6 Movie S9 within the Supplemental Material [48]). Despite the fact that small solitons cannot be clearly distinguished by the polarizing optical microscope, due to limited light intensity and optical resolution, the

larger ones have polarizing optical textures analogous to those obtained for pitch  $p \sim 2 \mu\text{m}$  [Figs. S2(a) and S5(a) within the Supplemental Material [48]]. Individual solitons undergo anomalous diffusion at low  $f$ , where both subdiffusion and superdiffusion are observed (Fig. S7 within the Supplemental Material [48]). Such behavior is attributed to the nonlinear coupling between backflow and the isotropic flow of ions. Directional collective motion of solitons is also observed, but is, however, significantly different from that mentioned above. In the case of  $p \sim 2 \mu\text{m}$ , the ionic flows and associated hydrodynamic effects are suppressed by using a high carrier frequency,  $f = 10\text{--}50$  kHz. The solitons move consistently in a specific direction with a constant velocity and a velocity-order parameter  $S = \left| \sum_i^N v_i \right| / (N v_s)$  close to one, where  $N$  is the number of solitons and  $v_s$  is the absolute value of the velocity of coherently moving solitons (Fig. S8 within the Supplemental Material [48]). In contrast, here, due to the isotropic flows of ions at low  $f$ , individual solitons move in different directions at each moment [Fig. 6(a)], with a much smaller velocity-order parameter,  $S \sim 0.4$  [Fig. 6(c)], and an average velocity of about  $-2 \mu\text{m s}^{-1}$ , pointing in the  $-y$  direction [Fig. 6(d)], induced by backflow (Movie S10 within the Supplemental Material [48]). Solitons undergo hydrodynamic fluctuations, leading to a locally meandering but long-term directed trajectory [Fig. 6(b)], which is very different from the smooth and straight trajectory shown in Fig. 5(a). Generally, active fluids exhibit behavior beyond the expectation of equilibrium statistical mechanics, such as so-called giant-number fluctuations (GNF). We analyze the relationship between the mean number,  $\langle N \rangle$ , and the root-mean-square number,  $\Delta N = \langle (N - \langle N \rangle)^2 \rangle^{1/2}$ , of solitons within different sample areas. Unlike the case of stochastic Brownian motion of colloidal particles, where  $\Delta N \propto \langle N \rangle^\beta$  with  $\beta = 1/2$  [65], the collective directional motion of solitons exhibits GNF with  $\beta = 1.13$  [Fig. 6(e)]. Figure 6(f) shows the evolution of fluctuations in the local number density analyzed by counting the numbers of solitons within a selected sample area of  $146 \times 130 \mu\text{m}^2$ . It is found that the density  $\eta$  decreases gradually and then saturates at a late stage, which is due to the coalescence of solitons at low  $f$  (Fig. S9 within the Supplemental Material [48]). The topological protection of skyrmions is caused by the swirling director texture and is strictly enforced in the continuum. Understanding the mechanism of unwinding skyrmions is vital to the enhancement of their stability [66]. Merging of skyrmions is reported in magnetic materials and is attributed to the proliferation and propagation of magnetic Bloch points [67]. In our case, such a coalescence may be attributed to the interactions between the hedgehog point defects or the fierce inelastic collisions among solitons that destroy the topologically protected structures. During motion, the solitons behave like colloidal

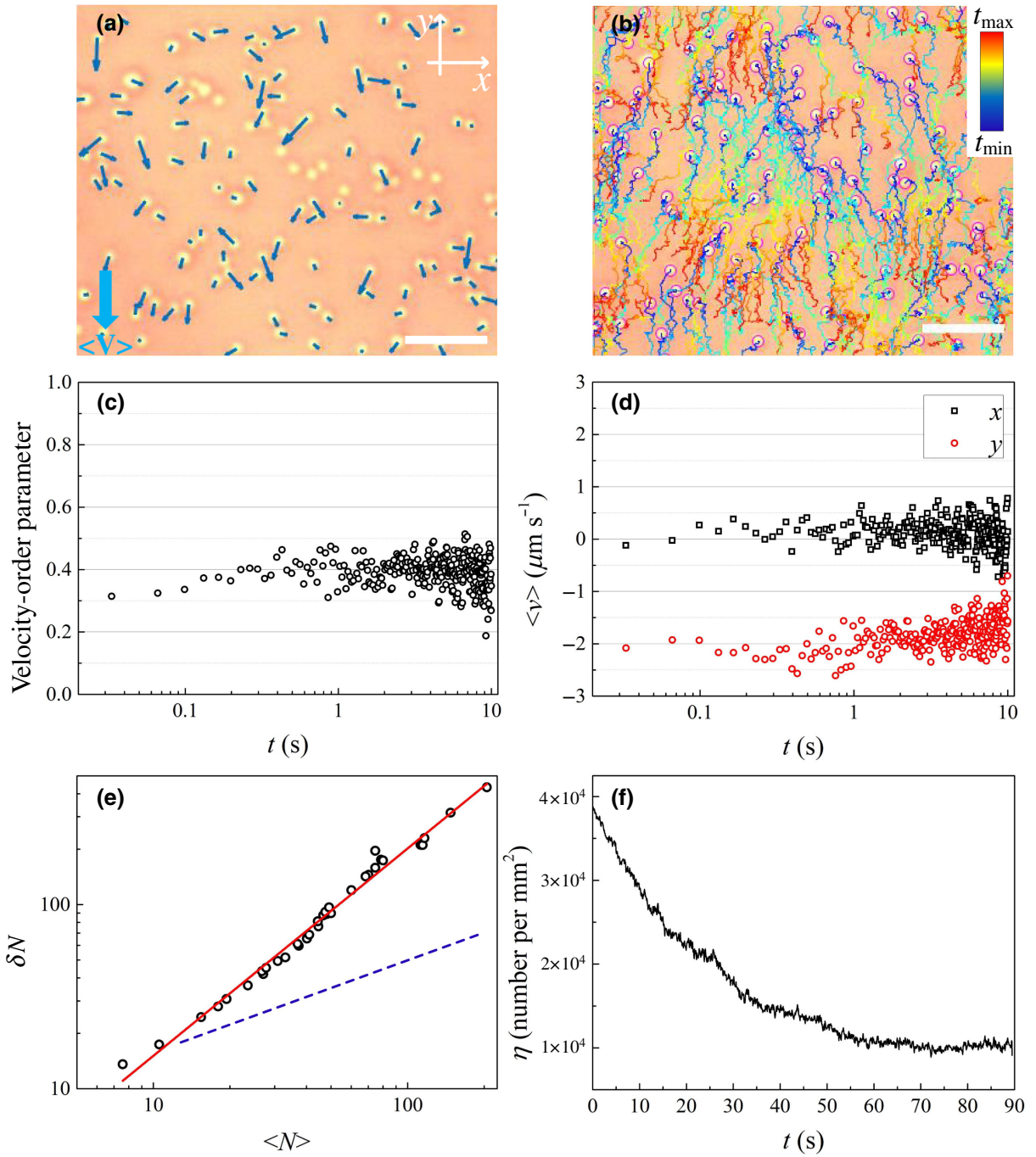


FIG. 6. Coherent skyrmionic soliton motion in CNLCs with pitch  $p \sim 0.375 \mu\text{m}$  confined in a cell with cell gap  $d = 5.0 \mu\text{m}$ . Micrograph of skyrmionic solitons at 0.5 s after applying an electric field (a) with their velocities marked as small blue arrows (amplitudes of velocities are indicated as the lengths of the arrows) and (b) with their trajectories over time, according to the color bar ( $t_{\min} = 0.5$  s,  $t_{\max} = 10$  s). Scale bars  $10 \mu\text{m}$ . Evolution of (c) velocity-order parameter and (d) average velocities of solitons in (a) with time. (e) Giant-number fluctuation analysis using  $\log_{10}$ - $\log_{10}$  plot of  $\Delta N$  versus  $\langle N \rangle$ ; red line is the linear fit of experimental data points (symbol); blue dashed line indicates a slope of 0.5 for reference. (f) Example of number-density fluctuation during motion for a  $146 \times 130 \mu\text{m}^2$  sample area.  $E = 5.0 \text{ V } \mu\text{m}^{-1}$ ,  $f = 200$  Hz for all measurements.

particles with a sticking probability of  $s < 1$ , forming anisotropic clusters while they collide. We describe the geometry of aggregated soliton clusters by their fractal dimensions (Fig. 7). Despite the limited number of clusters

measured (over 100 in our case), the fractal dimension still provides a reasonably accurate description of differences in the shape of clusters at different stages. We analyze the cluster structures by using the ‘‘inertia’’

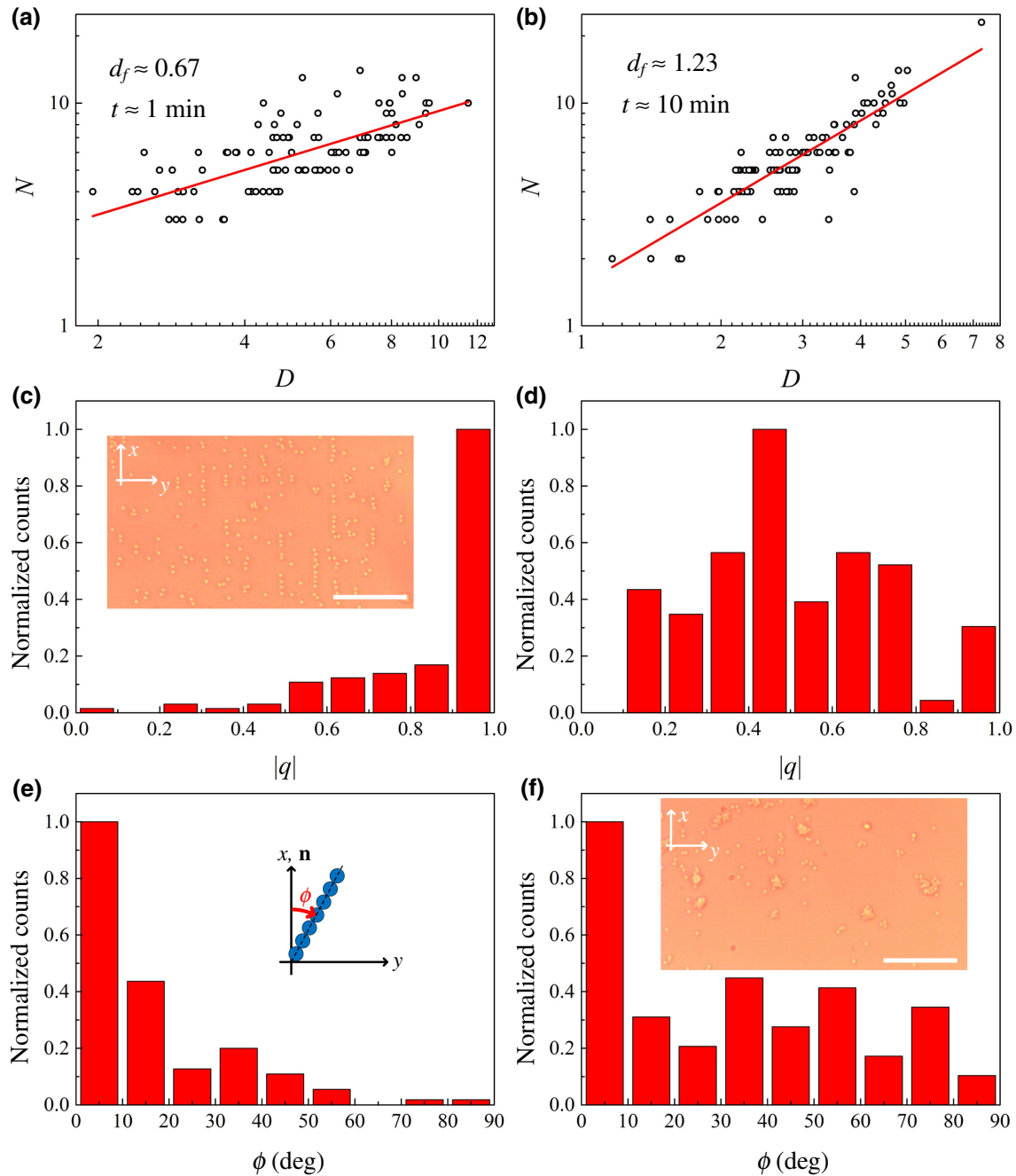


FIG. 7. Aggregation of skyrmionic solitons in CNLCs with pitch  $p \sim 0.375 \mu\text{m}$  confined in a cell with cell gap  $d = 5.0 \mu\text{m}$ .  $\text{Log}_{10}\text{-log}_{10}$  plot of number of solitons,  $N$ , and cluster diameter,  $D$ , at (a) 1 min and (b) 10 min after applying an electric field. Red lines are linear fits of experimental data points (symbol). Histograms of cluster anisotropy  $|q|$  at (c) 1 min and (d) 10 min after applying electric field. Histograms of the angle between the long axis of clusters and alignment direction ( $x$  axis)  $\phi$  at (e) 1 min and (f) 10 min after applying an electric field. Insets in (c) and (f) are micrographs of aggregates of solitons at 1 and 10 min after applying electric field, respectively. Scale bar  $30 \mu\text{m}$ .  $E = 4.88 \text{ V } \mu\text{m}^{-1}$ ,  $f = 200 \text{ Hz}$ .

tensor [68,69], which is defined for a cluster composed of  $N$  solitons as  $M_{ab} = \sum_{i=1}^N (\rho_a^i - \bar{\rho}_a)(\rho_b^i - \bar{\rho}_b)$ , where  $a, b = x, y$ ;  $\rho^i = (\rho_x^i, \rho_y^i)$  are coordinates of the  $i$ th soliton; and  $\bar{\rho} = N^{-1} \sum_{i=1}^N \rho^i$  is the center of mass of the cluster. This allows us to define a characteristic diameter,  $D = 2\sqrt{\text{Tr}M}/N$ , and anisotropy of individual clusters,

$q = (M_{xx} - M_{yy} + 2iM_{xy}) / (M_{yy} + M_{xx}) = |q|e^{i2\phi}$ , where  $|q|$  and  $\phi$  are the cluster's elongation and azimuthal angle of the long axis, respectively. It is  $|q| = 1$  for a stringlike cluster and  $|q| = 0$  for a disklike cluster [69]. Statistical analysis of the relationship between  $N$  and  $D$  reveals that clusters exhibit fractal behavior,  $N \propto D^{d_f}$ , where  $d_f$

denotes the Hausdorff dimension. Generally, a uniform object embedded in  $m$ -dimensional space has  $d_f = m$ , while a loose structure with decreasing density from its center has  $d_f < m$  [70]. It is found that the solitons form one-dimensional linear chains at the beginning, which are gradually destroyed by fluid flows and turn into irregular clusters at a later stage (Fig. 7).

### III. DISCUSSION

Recently, multidimensional dynamic dissipative solitons in nematics were reported by us [27,28] and other groups [25,26,29] and have attracted increasing attention due to their fascinating nonlinear dynamic behaviors and potential applications in microfluidic systems. These solitons can move with a velocity that is controllable by external electric fields. They preserve spatially confined shapes during motion and survive collisions, which is similar to the dynamics of the skyrmionic solitons described above. However, unlike skyrmionic solitons, the existence of which is topologically protected and guaranteed by the helicoidal structure of the cholesteric phase that maintains a fixed pitch, dissipative solitons are actually self-trapped propagating solitary waves of director deformations and are thus topologically trivial and equivalent to the uniform state. They are formed by the flexoelectric effect of LC molecules and nonlinear coupling between the electrohydrodynamic flows and the LC director field. They require an external driving force to exist, such as that provided by applied electric fields.

In previous studies [11,34,52,62], skyrmionic solitons usually emerged between boundaries with homeotropic alignment, as a result of geometrical frustration between surface anchoring and material chirality. In the same mechanism, skyrmions can also be formed in cells with homogeneous alignment, where their stability is supported by the subtle balance between chirality and the electric field. Such a configuration facilitates dynamic field control of the geometrical transformation of skyrmions. A variety of patterns can be formed in frustrated CNLCs with positive dielectric anisotropy by applying an electric field. Moreover, a first-order cholesteric-nematic transition [71] can be achieved by increasing the electric field to completely unwind the helical structures, so that there is a coexistence line in the parameter plane, where the two phases have exactly the same elastic energy and coexist [71]. Just below this line, different kinds of cholesteric fingers can form, depending on various parameters, including  $d/p$  and  $E$ . CF2s, as one of the most common types of finger, have a topological structure analogous to skyrmions [72]. There are point defects near each end of a CF2, which are not at the same height but are localized near the two substrates [71]. By increasing  $E$  just above the coexistence line, a CF2 continuously shortens until a toron is formed. On the other hand, it was reported that closed

loops of a CF1 could form skyrmionic solitons, while a looped CF2 never formed such solitons unless it possessed point defects [44]. More importantly, such a transformation from looped CF2 to skyrmionic solitons has never been reported to be reversible. These discrepancies from our results may be attributed to the extraordinarily large value of  $d/p$  in our case. In previous studies [11,37,52,71], depending on the elastic constants of LC materials, there is a very strict requirement on  $d/p$  (generally speaking,  $d/p \sim 1$ ) to achieve the fragile balance between twist energy and homeotropic anchoring. This also greatly limits investigations into topological solitons in high-chirality systems, where, apart from the coalescence of solitons, complicated dynamic motions, giant-number fluctuations, or anisotropic clusters that we report here, other interesting phenomena, such as half-skyrmions [73], may also be found.

Although the collective directional motion of skyrmionic solitons in LCs has been reported recently [57,74], the influence of fluid flows has not been discussed yet. Furthermore, controlling the dynamic motion of solitons has never really been achieved before. We find that the solitons in our experiments always move perpendicular to the alignment direction and can be continuously switched to the opposite direction by tuning the electric field, owing to the effects of backflow. Backflow has been notorious in LC display applications for decades, as it causes flickering of display pixels. However, as an effect, it has begun to gain popularity in recent years due to its broad applications in microfluidics, such as non-Stokesian dynamics of colloidal particles [75], inelastic collision and aggregation of colloidal particles [68], and annihilation dynamics of topological defects [64]. By tuning the alignment condition and the value of  $d/p$ , we may change the velocity profile of backflows [61], and thus, vary the dynamic motion of the solitons. We also demonstrate that 2D micromanipulation of the dynamics of solitons can be realized by predesigned patterned alignment. With the help of the photoalignment technique [63], various motions, such as spiral motion, wavy motion, and zigzag motion, can be achieved, which will be reported elsewhere. Since the skyrmionic solitons interact with colloidal microparticles, as shown, this enables various forms of cargo transport on micrometer scales.

### IV. CONCLUSION

We demonstrate the dynamic formation of skyrmionic solitons in CNLCs with varied pitches confined between surfaces with homogeneous anchoring. The field-induced reversible transformations from cholesteric fingers to topological solitons overcome the restraint on the value of  $d/p$ , and thus, facilitate investigations into systems of high chirality. Stable skyrmion bags with a field-controllable topological degree are generated spontaneously, which

may be utilized as models of atomic nuclei with different baryon numbers or even for potential applications such as ultrahigh-density optical or magnetic information storage systems. Solitons undergo anomalous diffusion at equilibrium and perform collective directional motion in response to modulated electric fields attributed to the effects of back-flow. The 2D micromanipulation and microcargo transport can be achieved through predesigned alignment. Nonlinear coupling with isotropic ion flows at low frequency induces complex superdiffusion of individual solitons and coherent meandering of hundreds and thousands of solitons. The solitons collide like colloidal particles and form anisotropic clusters. Our findings fill the missing pieces in the study of out-of-equilibrium phenomena of topological solitons and open avenues for versatile dynamic soliton systems with potential applications in microfluidics and racetrack memory devices.

## ACKNOWLEDGMENTS

Y.S. would like to acknowledge the China Scholarship Council (CSC) for funding.

## APPENDIX: EXPERIMENTAL METHODS

### 1. Sample preparation

The CNLCs used are prepared by mixing a commercially available nematic liquid crystal, E7 (Xianhua, China), with chiral dopants. Different pitches are obtained by varying the concentration,  $c$ , of chiral dopants, according to the relationship  $p = 1/(Hc)$ , where  $H$  represents the helical twisting power of the chiral dopant. The CNLCs with pitch  $p \sim 2.0$  and  $5.0 \mu\text{m}$  are prepared with chiral dopant S811 (ZLI-811) (Xianhua, China), the  $H$  of which is  $-10.9 \mu\text{m}^{-1}$  [28], and the CNLC with  $p \sim 0.375 \mu\text{m}$  is prepared with chiral dopant R5011 (Xianhua, China), which has a much larger  $H$  of about  $110 \mu\text{m}^{-1}$  [76]. The small pitch,  $p \sim 0.375 \mu\text{m}$ , is further verified by measuring the Bragg reflection of the sample, as shown in Fig. S10 within the Supplemental Material [48]. It is well known that the CNLC can Bragg reflect circularly polarized light with the same handedness as that of its chiral structure due to its characteristic helical superstructure [77]. The wavelength of reflected light is dependent on the ordinary ( $n_o$ ) and extraordinary ( $n_e$ ) refractive indices and the pitch,  $p$ , of the CNLC as  $\bar{\lambda} = \bar{n}p$ , where  $\bar{\lambda}$  is the average wavelength of the reflected light band and  $\bar{n} = (1/2)(n_o + n_e)$  is the average refractive index [77]. According to Ref. [76], the refractive indices of E7 at  $\lambda = 633 \text{ nm}$  and  $T = 20^\circ\text{C}$  are  $n_o = 1.517$  and  $n_e = 1.741$ . We measure that  $\bar{\lambda} \sim 611 \text{ nm}$  (Fig. S10 within the Supplemental Material [48]), and thus, obtain  $p \sim 375 \text{ nm}$ , which is in accordance with the calculation. However, it should be noted that, because the refractive indices of E7 in Ref. [76] do not exactly match the temperature of our system, there

could be a slight difference between the calculated pitch and the real pitch. LC cells coated with rubbed polyimide are purchased from AWAT (Poland). LC cells processed by the photoalignment technique are composed of two glass substrates coated with transparent indium tin oxide (ITO) layers. The glass substrates are first ultrasonically bathed, plasma cleaned, and then spin-coated with a 0.3 wt% dimethylformamide solution of sulfonic azo dye SD1 (Dai-Nippon Ink and Chemicals, Japan). The substrates are glued together, and the cell gap is set with spacers. The cell gap is measured by the thin-film interference method [78]. Afterwards, the empty cells are illuminated by polarized ultraviolet light with wavelength  $\lambda = 395 \text{ nm}$ . Finally, LC mixtures are heated to the isotropic phase and fill the cells through capillary action.

### 2. Generation of solitons

Samples are kept at  $50^\circ\text{C}$  on a hot stage (LTSE350, Linkam) controlled by a temperature controller (TP 94, Linkam). The ac voltage is applied using a waveform generator (33220A, Agilent) and a home-built amplifier.

### 3. Optical characterization

Samples are observed through a polarizing microscope (Leica OPTIPOL). Images and movies are recorded by using a charge-coupled device camera (UI-3360CP-C-HQ, uEye Gigabit Ethernet). In the measurements of Brownian motion, the frame rate of the camera is tuned to 100 frames/s and each sample is tracked by the camera for 5 min, which gives, overall, 30 000 trajectory steps for each measurement.

### 4. Data analysis

The motion of the solitons is tracked and analyzed by using open-source ImageJ and Fiji software. The position information and number density of the solitons are extracted for each frame through a plugin of ImageJ, TrackMate. The temporal evolution of velocity order is obtained by analyzing the positional information of solitons between frames of movies. The giant-number fluctuations are analyzed by analyzing the soliton number density versus time for 35 areas of different sizes, ranging from  $30 \times 25$  to  $180 \times 145 \mu\text{m}^2$ .

- 
- [1] T. Dauxois and M. Peyrard, *Physics of Solitons* (Cambridge University Press, Cambridge, 2006).
  - [2] Y. V. Kartashov, G. E. Astrakharchik, B. A. Malomed, and L. Torner, Frontiers in multidimensional self-trapping of nonlinear fields and matter, *Nat Rev. Phys.* **1**, 185 (2019).
  - [3] N. Manton and P. Sutcliffe, *Topological Solitons* (Cambridge University Press, Cambridge, 2004).

- [4] Y. M. Shnir, *Topological and non-Topological Solitons in Scalar Field Theories* (Cambridge University Press, Cambridge, 2018).
- [5] L. H. Kauffman, *Knots and Physics* (World scientific, Singapore, 2001), Vol. 1.
- [6] T. H. R. Skyrme, A unified field theory of mesons and baryons, *Nucl. Phys.* **31**, 556 (1962).
- [7] T. H. R. Skyrme, in *Selected Papers, With Commentary, Of Tony Hilton Royle Skyrme* (World Scientific, London, 1994), pp. 195.
- [8] S. Mühlbauer, B. Binz, F. Jonietz, C. Pfleiderer, A. Rosch, A. Neubauer, R. Georgii, and P. Boni, Skyrmion lattice in a chiral magnet, *Science* **323**, 915 (2009).
- [9] X. Yu, Y. Onose, N. Kanazawa, J. H. Park, J. H. Han, Y. Matsui, N. Nagaosa, and Y. Tokura, Real-space observation of a two-dimensional skyrmion crystal, *Nature* **465**, 901 (2010).
- [10] A. N. Bogdanov, U. K. Röbner, and A. A. Shestakov, Skyrmions in nematic liquid crystals, *Phys. Rev. E* **67**, 016602 (2003).
- [11] I. I. Smalyukh, Y. Lansac, N. A. Clark, and R. P. Trivedi, Three-dimensional structure and multistable optical switching of triple-twisted particle-like excitations in anisotropic fluids, *Nat. Mater.* **9**, 139 (2009).
- [12] S. Krause and R. Wiesendanger, Skyrmionics gets hot, *Nat. Mater.* **15**, 493 (2016).
- [13] W. E. L. Haas and J. E. Adams, New optical storage mode in liquid crystals, *Appl. Phys. Lett.* **25**, 535 (1974).
- [14] A. Varanytsia and L.-C. Chien, Photoswitchable and dyedoped bubble domain texture of cholesteric liquid crystals, *Opt. Lett.* **40**, 4392 (2015).
- [15] A. Varanytsia, G. Posnjak, U. Mur, V. Joshi, K. Darrah, I. Musevic, S. Copar, and L.-C. Chien, Topology-commanded optical properties of bistable electric-field-induced torons in cholesteric bubble domains, *Sci. Rep.* **7**, 1 (2017).
- [16] W. Helfrich, Alignment-Inversion Walls in Nematic Liquid Crystals in the Presence of a Magnetic Field, *Phys. Rev. Lett.* **21**, 1518 (1968).
- [17] L. Leger, Observation of wall motions in nematics, *Solid State Commun.* **10**, 697 (1972).
- [18] K. B. Migler and R. B. Meyer, Solitons and Pattern Formation in Liquid Crystals in a Rotating Magnetic Field, *Phys. Rev. Lett.* **66**, 1485 (1991).
- [19] T. Frisch, S. Rica, P. Coulet, and J. M. Gilli, Spiral Waves in Liquid Crystal, *Phys. Rev. Lett.* **72**, 1471 (1994).
- [20] C. Zheng and R. B. Meyer, Thickness effects on pattern formation in liquid crystals in a rotating magnetic field, *Phys. Rev. E* **55**, 2882 (1997).
- [21] L. Lei, C. Q. Shu, J. L. Shen, P. M. Lam, and Y. Huang, Soliton Propagation in Liquid Crystals, *Phys. Rev. Lett.* **49**, 1335 (1982).
- [22] Z. Guozhen, Experiments on Director Waves in Nematic Liquid Crystals, *Phys. Rev. Lett.* **49**, 1332 (1982).
- [23] L. Lei, S. Changqing, and X. Gang, Generation and detection of propagating solitons in shearing liquid crystals, *J. Stat. Phys.* **39**, 633 (1985).
- [24] M. Peccianti and G. Assanto, Nematicons, *Phys. Rep.* **516**, 147 (2012).
- [25] B.-X. Li, V. Borshch, R. L. Xiao, S. Paladugu, T. Turiv, S. V. Shiyankovskii, and O. D. Lavrentovich, Electrically driven three-dimensional solitary waves as director bullets in nematic liquid crystals, *Nat. Commun.* **9**, 2912 (2018).
- [26] B.-X. Li, R. L. Xiao, S. Paladugu, S. V. Shiyankovskii, and O. D. Lavrentovich, Three-dimensional solitary waves with electrically tunable direction of propagation in nematics, *Nat. Commun.* **10**, 3749 (2019).
- [27] Y. Shen and I. Dierking, Dynamics of electrically driven solitons in nematic and cholesteric liquid crystals, *Commun. Phys.* **3**, 1 (2020).
- [28] Y. Shen and I. Dierking, Dynamic dissipative solitons in nematics with positive anisotropies, *Soft Matter* **16**, 5325 (2020).
- [29] S. Aya and F. Araoka, Kinetics of motile solitons in nematic liquid crystals, *Nat. Commun.* **11**, 3248 (2020).
- [30] P.-G. De Gennes and J. Prost, *The Physics of Liquid Crystals (2nd Edition)* (Oxford University Press, New York, 1993), Vol. 83.
- [31] Y. Shen and I. Dierking, Perspectives in liquid-crystal-aided nanotechnology and nanoscience, *Appl. Sci.* **9**, 2512 (2019).
- [32] R. D. Kamien and J. V. Selinger, Order and frustration in chiral liquid crystals, *J. Phys.: Condens. Matter* **13**, R1 (2001).
- [33] P. Oswald, J. Baudry, and S. Pirkl, Static and dynamic properties of cholesteric fingers in electric field, *Phys. Rep.* **337**, 67 (2000).
- [34] B. Kerllenevich and A. Coche, Bubble domain in cholesteric liquid crystals, *Mol. Cryst. Liq. Cryst.* **68**, 47 (1981).
- [35] P. J. Ackerman, R. P. Trivedi, B. Senyuk, J. V. D. Lagemaat, and I. I. Smalyukh, Two-dimensional skyrmions and other solitonic structures in confinement-frustrated chiral nematics, *Phys. Rev. E* **90**, 012505 (2014).
- [36] S. Afghah and J. V. Selinger, Theory of helicoids and skyrmions in confined cholesteric liquid crystals, *Phys. Rev. E* **96**, 012708 (2017).
- [37] P. J. Ackerman, J. van de Lagemaat, and I. I. Smalyukh, Self-assembly and electrostriction of arrays and chains of hopfion particles in chiral liquid crystals, *Nat. Commun.* **6**, 6012 (2015).
- [38] P. J. Ackerman and I. I. Smalyukh, Diversity of Knot Solitons in Liquid Crystals Manifested by Linking of Preimages in Torons and Hopfions, *Phys. Rev. X* **7**, 011006 (2017).
- [39] P. J. Ackerman, T. Boyle, and I. I. Smalyukh, Squirming motion of baby skyrmions in nematic fluids, *Nat. Commun.* **8**, 673 (2017).
- [40] S. Woo, K. Litzius, B. Kruger, M.-Y. Im, L. Caretta, K. Richter, M. Mann, A. Krone, R. M. Reeve, M. Weigand, P. Agrawal, I. Lemesh, M.-A. Mawass, P. Fischer, M. Klau, and G. S. D. Beach, Observation of room-temperature magnetic skyrmions and their current-driven dynamics in ultrathin metallic ferromagnets, *Nat. Mater.* **15**, 501 (2016).
- [41] F. Zheng, F. N. Rybakov, A. B. Borisov, D. Song, S. Wang, Z. Li, H. Du, N. S. Kiselev, J. Caron, A. Kovacs, M. Tian, Y. Zhang, S. Blugel, and R. E. D. Borkowski, Experimental observation of chiral magnetic bobbers in B20-type FeGe, *Nat. Nanotechnol.* **13**, 451 (2018).
- [42] M. Kleman and O. D. Lavrentovich, *Soft Matter Physics: an Introduction* (Springer Science & Business Media, New York, 2007).

- [43] S.-S. Li, Y. Shen, Z. N. Chang, W. S. Li, Y. C. Xu, X. Y. Fan, and L. J. Chen, Dynamic cholesteric liquid crystal superstructures photoaligned by one-step polarization holography, *Appl. Phys. Lett.* **111**, 231109 (2017).
- [44] J. Baudry, S. Pirkel, and P. Oswald, Looped finger transformation in frustrated cholesteric liquid crystals, *Phys. Rev. E* **59**, 5562 (1999).
- [45] J. Baudry, S. Pirkel, and P. Oswald, Topological properties of singular fingers in frustrated cholesteric liquid crystals, *Phys. Rev. E* **57**, 3038 (1998).
- [46] L. Gil and J. M. Gilli, Surprising Dynamics of Some Cholesteric Liquid Crystal Patterns, *Phys. Rev. Lett.* **80**, 5742 (1998).
- [47] P. Ribière, P. Oswald, and S. Pirkel, Crawling and spiraling of cholesteric fingers in electric field, *J. de Phys. II* **4**, 127 (1994).
- [48] See the Supplemental Material at <http://link.aps.org/supplemental/10.1103/PhysRevApplied.15.054023> for supplementary figures, table, and movies.
- [49] D. Foster, C. Kind, P. J. Ackerman, J. S. B. Tai, M. R. Dennis, and I. I. Smalyukh, Two-dimensional skyrmion bags in liquid crystals and ferromagnets, *Nat. Phys.* **15**, 655 (2019).
- [50] A. Fert, V. Cros, and J. Sampaio, Skyrmions on the track, *Nat. Nanotechnol.* **8**, 152 (2013).
- [51] C. Loussert and E. Brasselet, Multiple chiral topological states in liquid crystals from unstructured light beams, *Appl. Phys. Lett.* **104**, 051911 (2014).
- [52] J.-S. B. Tai and I. I. Smalyukh, Surface anchoring as a control parameter for stabilizing torons, skyrmions, twisted walls, fingers, and their hybrids in chiral nematics, *Phys. Rev. E* **101**, 042702 (2020).
- [53] W. B. Russel, *et al.*, *Colloidal Dispersions* (Cambridge university press, Cambridge, 1991).
- [54] W. Coffey and Y. P. Kalmykov, *The Langevin Equation: with Applications to Stochastic Problems in Physics, Chemistry and Electrical Engineering* (World Scientific, New Jersey, 2012), Vol. 27.
- [55] V. Kenkre, R. Kühne, and P. Reineker, Connection of the velocity autocorrelation function to the mean-square-displacement and to the memory function of generalized master equations, *Zeitschrift für Physik B Condensed Matter* **41**, 177 (1981).
- [56] T. Turiv, I. Lazo, A. Brodin, B. I. Lev, V. Reiffenrath, V. G. Nazarenko, and O. D. Lavrentovich, Effect of collective molecular reorientations on brownian motion of colloids in nematic liquid crystal, *Science* **342**, 1351 (2013).
- [57] H. R. O. Sohn, C. D. Liu, and I. I. Smalyukh, Schools of skyrmions with electrically tunable elastic interactions, *Nat. Commun.* **10**, 4744 (2019).
- [58] S. Palagi, A. G. Mark, S. Y. Reigh, K. Melde, T. Qiu, H. Zeng, C. Parmeggiani, D. Martella, A. S. Castillo, N. Kapernaum, F. Giesselmann, D. S. Wiersma, E. Lauga, and P. Fischer, Structured light enables biomimetic swimming and versatile locomotion of photoresponsive soft microrobots, *Nat. Mater.* **15**, 647 (2016).
- [59] Ž Kos and M. Ravnik, Field generated nematic microflows via backflow mechanism, *Sci. Rep.* **10**, 1446 (2020).
- [60] K. Xiao, X. Chen, and C.-X. Wu, Fréedericksz-Like Positional Transition, *Phys. Rev. Res.* **1**, 033041 (2019).
- [61] Y. Mieda and K. Furutani, Two-dimensional micromanipulation using liquid crystals, *Appl. Phys. Lett.* **86**, 101901 (2005).
- [62] M. Kawachi, O. Kogure, and Y. Kato, Bubble domain texture of a liquid crystal, *Jpn. J. Appl. Phys.* **13**, 1457 (1974).
- [63] Y. Shen, Y. C. Xu, Y. H. Ge, R. G. Jiang, X. Z. Wang, S. S. Li, and L. J. Chen, Photoalignment of dye-doped cholesteric liquid crystals for electrically tunable patterns with fingerprint textures, *Opt. Express* **26**, 1422 (2018).
- [64] Y. Shen and I. Dierking, Annihilation dynamics of topological defects induced by microparticles in nematic liquid crystals, *Soft Matter* **15**, 8749 (2019).
- [65] V. Narayan, S. Ramaswamy, and N. Menon, Long-Lived giant number fluctuations in a swarming granular nematic, *Science* **317**, 105 (2007).
- [66] F. Muckel, S. V. Malotki, C. Holl, B. Pestka, M. Pratzner, P. F. Bessarab, S. Heinze, and M. Morgenstern, Experimental identification of two distinct skyrmion collapse mechanisms, *Nat. Phys.* **17**, 395 (2021).
- [67] P. Milde, D. Kohler, J. Seidel, L. M. Eng, A. Bauer, A. Chacon, J. Kindervater, S. Muhlbauer, C. Pfleiderer, S. Buhrandt, C. Schutte, and A. Rosch, Unwinding of a skyrmion lattice by magnetic monopoles, *Science* **340**, 1076 (2013).
- [68] O. P. Pishnyak, S. V. Shiyankovskii, and O. D. Lavrentovich, Inelastic Collisions and Anisotropic Aggregation of Particles in a Nematic Collider Driven by Backflow, *Phys. Rev. Lett.* **106**, 047801 (2011).
- [69] O. P. Pishnyak, S. V. Shiyankovskii, and O. D. Lavrentovich, Aggregation of colloidal particles in a non-equilibrium backflow induced by electrically-driven reorientation of the nematic liquid crystal, *J. Mol. Liq.* **164**, 132 (2011).
- [70] D. W. Schaefer, J. E. Martin, P. Wiltzius, and D. S. Cannell, Fractal Geometry of Colloidal Aggregates, *Phys. Rev. Lett.* **52**, 2371 (1984).
- [71] S. Pirkel, Time evolution of cholesteric fingers of the second species in an electric field, *Cryst. Res. Technol.* **44**, 1323 (2009).
- [72] S. Pirkel, P. Ribiere, and P. Oswald, Forming process and stability of bubble domains in dielectrically positive cholesteric liquid crystals, *Liq. Cryst.* **13**, 413 (1993).
- [73] A. Nych, J. I. Fukuda, U. Ognysta, S. Zumer, and I. Musevic, Spontaneous formation and dynamics of half-skyrmions in a chiral liquid-crystal film, *Nat. Phys.* **13**, 1215 (2017).
- [74] H. R. Sohn and I. I. Smalyukh, Electrically powered motions of toron crystallites in chiral liquid crystals, *Proc. Natl. Acad. Sci. U. S. A.* **117**, 6437 (2020).
- [75] O. P. Pishnyak, S. Tang, J. R. Kelly, S. V. Shiyankovskii, O. D. Lavrentovich, and Lift Levitation, And Bidirectional Motion of Colloidal Particles in an Electrically Driven Nematic Liquid Crystal, *Phys. Rev. Lett.* **99**, 127802 (2007).
- [76] K.-J. Che, Y. J. Yang, Y. L. Lin, Y. W. Shan, Y. H. Ge, S. S. Li, L. J. Chen, and C. Y. J. Yang, Microfluidic generation of cholesteric liquid crystal droplets with an integrative cavity for dual-gain and controllable lasing, *Lab Chip* **19**, 3116 (2019).
- [77] N. H. Hartshorne, *The Microscopy of Liquid Crystals* (Microscope Publications Ltd., London, 1974).
- [78] A. M. Goodman, Optical interference method for the approximate determination of refractive index and thickness of a transparent layer, *Appl. Opt.* **17**, 2779 (1978).